

Charm and bottom photoproduction at HERA with MC@NLO

T. Toll

Physics Department, Brookhaven National Laboratory, Upton, NY 11973, USA

S. Frixione

*PH Department, TH Unit, CERN, CH-1211 Geneva 23, Switzerland
ITPP, EPFL, CH-1015 Lausanne, Switzerland*

Abstract

We apply the MC@NLO formalism to the production of heavy-quark pairs in pointlike photon-hadron collisions. By combining this result with its analogue relevant to hadron-hadron collisions, we obtain NLO predictions matched to parton showers for the photoproduction of $Q\bar{Q}$ pairs. We compare MC@NLO results to the measurements of c - and b -flavoured hadron observables performed by the H1 and ZEUS collaborations at HERA

Keywords: MC@NLO, heavy quarks, photoproduction

1. Introduction

The production of pairs of quarks with mass much larger than the typical hadronic scale, thus called heavy, has distinctive features that renders it an interesting case study. From the theoretical viewpoint, the quark mass cuts the collinear singularities off, and open-quark cross sections, in which no fragmentation functions or jet-finding algorithms are used, are well defined in perturbation theory. On the experimental side, heavy-quark production can be exploited thanks to its peculiar signatures, and generally large rates. The definition of what is heavy is to a certain extent ambiguous, and may depend on the kinematic region one is interested into probing (since the behaviour of a particle with mass m can be fairly different according to whether $m \gg p_T$ or $m \ll p_T$). While there is no doubt that the top is heavy, the heaviness of the bottom quark may be debatable, and that of the charm quark certainly is. It remains true, however, that open charm and bottom cross sections can be computed at fixed order in QCD; the interesting question is therefore how predictions compare to data.

Email addresses: ttoll@bnl.gov (T. Toll), Stefano.Frixione@cern.ch (S. Frixione)

This question has indeed received a lot of attention in the past twenty years, in part because of the important role played by heavy quarks in many discovery channels of BSM physics. Apart from the mainstream activity at hadron machines, the ep collider HERA has also been collecting charm and bottom data for over a decade now, in both the DIS and the photoproduction regimes (see e.g. ref [1] for a review). With its relatively small c.m. energy of about 300 GeV, heavy-quark physics at HERA very rarely involves large transverse momenta, and therefore offers a good testing ground for purely-perturbative QCD predictions. It is now customary to compare data to results accurate to NLO ($\mathcal{O}(\alpha_{em}\alpha_S^2)$) [1]; fully exclusive computations, in both DIS [2] and photoproduction [3], have been available for some time now.

Comparisons between data and parton-level, fixed-order predictions are not entirely satisfactory. They may work well for fully inclusive observables dominated by hard scales, but unfortunately experimental measurements typically involve hadron-level, smallish-scale quantities which cannot be well described by such a simple theoretical framework, and corrections (which introduce biases) need be applied to theoretical results, data, or both, in this way blurring the picture. Parton Shower Monte Carlos (PSMCs) offer a viable alternative, with their fully realistic final states, but lack the accuracy of higher-order perturbative computations. The solution to the problem of matching the two approaches has been extensively studied in the past ten years, and is now fairly well established (see e.g. ref. [4] for a pedagogical introduction).

The purpose of this paper is that of applying the MC@NLO matching formalism [5] to the case of heavy-quark pair photoproduction, and of comparing the (hadron-level) results obtained in this way with selected bottom and charm measurements performed by the H1 and ZEUS collaborations at HERA. This paper is organized as follows: in sect. 2 we give the briefest introduction to the photoproduction jargon; in sect. 3 we summarize a few technical information on MC@NLO, specific to photon-initiated processes. Section 4 presents the comparisons between theoretical predictions and data; finally, in sect. 5 we report our conclusions.

2. Photoproduction: generalities

The high-energy photons that initiate photoproduction processes are typically obtained by quasi-collinear bremsstrahlung off an electron beam. We write the factorization theorem relevant to photoproduction as follows:

$$\begin{aligned} d\sigma_{eH} &= \sum_b \int dx_1 dx_2 f_\gamma^{(e)}(x_1) f_b^{(H)}(x_2) d\sigma_{\gamma b}(x_1, x_2) \\ &+ \sum_{ab} \int dx_1 dx_2 f_a^{(e)}(x_1) f_b^{(H)}(x_2) d\sigma_{ab}(x_1, x_2). \end{aligned} \quad (1)$$

We have denoted by $f_\gamma^{(e)}$ the Weizsäcker-Williams function [6, 7], which gives a good approximation of the energy spectrum of photons radiated by the electrons

(for the computations of this paper, we have used the form presented in ref. [8]). The functions $f_a^{(e)}$, the electron PDFs, are the analogues of the hadron PDFs, and are defined as follows:

$$f_a^{(e)}(x) = \int dy dz \delta(x - yz) f_\gamma^{(e)}(y) f_a^{(\gamma)}(z), \quad (2)$$

with $f_a^{(\gamma)}$ the relevant photon PDFs. The two terms on the r.h.s. of eq. (1) are usually called the pointlike and the hadronic photon components respectively. As the name suggests, the hadronic component is computed in exactly the same way as any ordinary hadron-hadron cross section. MC@NLO is no exception to this rule, and we have therefore used the calculation of ref. [9], with trivial modifications in the corresponding computer code that allow the use of electron PDFs. In this work, we have performed the computation of the pointlike contribution to $Q\bar{Q}$ production in MC@NLO. The underlying partonic processes are:

$$\gamma + g \longrightarrow Q + \bar{Q}, \quad (3)$$

$$\gamma + g \longrightarrow Q + \bar{Q} + g, \quad (4)$$

$$\gamma + q \longrightarrow Q + \bar{Q} + q, \quad (5)$$

where eq. (3) receives contributions from the Born ($\mathcal{O}(\alpha_{em}\alpha_s)$) and one-loop ($\mathcal{O}(\alpha_{em}\alpha_s^2)$) matrix elements, and eqs. (4)–(5) receive contributions from the real-emission matrix elements ($\mathcal{O}(\alpha_{em}\alpha_s^2)$), and from the corresponding counterterms as defined by the subtraction formalism adopted for the pure-NLO computation [3]. The matrix elements have been taken from ref. [3], which we have subsequently matched to fortran HERWIG [10, 11, 12], according to the MC@NLO formalism as described in the following section.

3. MC@NLO for $Q\bar{Q}$ photoproduction

The MC@NLO formalism has been introduced in ref. [5], and applied since then to a fairly large number of hadroproduction processes. The relevant technical details can be easily found in the literature, and we shall therefore refrain from giving them again here. We limit ourselves to recall that in the context of MC@NLO the matching of an NLO computation with a PSMC requires one to modify the short-distance cross sections that enter the former, with the inclusion of the so-called Monte Carlo (MC) subtraction terms, that are responsible for removing any double counting at the NLO. In turn, the MC subtraction terms have a factorized structure, being essentially constructed with Born-level cross sections and with process-independent branching kernels, which can be computed once and for all once the PSMC is chosen that will be used in the shower phase.

In order to determine the right combination of the Born matrix elements and branching kernels that enter the MC subtraction terms for a given production process, one formally expands the all-order PSMC cross sections to NLO. The

way in which the results so obtained are manipulated to construct the MC subtraction terms used in computer programmes is straightforward, and has been described in several papers. Here, we only give the results for the perturbative expansion mentioned above. Given the similarity between heavy-quark photo- and hadroproduction, we adopt the same notation as in ref. [9], where the latter process was studied. The PSMC cross sections read:

$$d\sigma\Big|_{\text{MC}} = \sum_b \sum_L \sum_l d\sigma_{eb}^{(L,l)}\Big|_{\text{MC}}, \quad (6)$$

where the first sum in eq. (6) runs over real-emission parton processes, eqs. (4) and (5). The index L runs over the emitting legs and it assumes the values $+$, $-$, Q , and \bar{Q} . The index l runs over the colour structures, and it can take the values t and u (clearly, there is no s -channel colour connection in the case of photoproduction). Following ref. [9], we obtain

$$d\sigma_{eb}^{(+,l)}\Big|_{\text{MC}} = \frac{1}{z_+^{(l)}} f_\gamma^{(e)}(\bar{x}_{1i}/z_+^{(l)}) f_b^{(H)}(\bar{x}_{2i}) d\hat{\sigma}_{\gamma g}^{(+,l)}\Big|_{\text{MC}} d\bar{x}_{1i} d\bar{x}_{2i}, \quad (7)$$

$$d\sigma_{eb}^{(-,l)}\Big|_{\text{MC}} = \frac{1}{z_-^{(l)}} f_\gamma^{(e)}(\bar{x}_{1i}) f_b^{(H)}(\bar{x}_{2i}/z_-^{(l)}) d\hat{\sigma}_{\gamma g}^{(-,l)}\Big|_{\text{MC}} d\bar{x}_{1i} d\bar{x}_{2i}, \quad (8)$$

$$d\sigma_{eg}^{(Q,l)}\Big|_{\text{MC}} = f_\gamma^{(e)}(\bar{x}_{1f}) f_b^{(H)}(\bar{x}_{2f}) d\hat{\sigma}_{\gamma g}^{(Q,l)}\Big|_{\text{MC}} d\bar{x}_{1f} d\bar{x}_{2f}, \quad (9)$$

$$d\sigma_{eg}^{(\bar{Q},l)}\Big|_{\text{MC}} = f_\gamma^{(e)}(\bar{x}_{1f}) f_b^{(H)}(\bar{x}_{2f}) d\hat{\sigma}_{\gamma g}^{(\bar{Q},l)}\Big|_{\text{MC}} d\bar{x}_{1f} d\bar{x}_{2f}. \quad (10)$$

These equations are identical to eqs. (5.2)–(5.5) of ref. [9], apart from the obvious notational changes due to the incoming electron in place of a hadron. The short distance cross sections in eqs. (7)–(10) are:

- γg initial state ($l = t, u$)

$$d\hat{\sigma}_{\gamma g}^{(-,l)}\Big|_{\text{MC}} = \frac{\alpha_s}{4\pi} \frac{d\xi_-^{(l)}}{\xi_-^{(l)}} dz_-^{(l)} P_{gg}^{(0)}(z_-^{(l)}) d\bar{\sigma}_{\gamma g} \Theta\left((z_-^{(l)})^2 - \xi_-^{(l)}\right), \quad (11)$$

$$d\hat{\sigma}_{\gamma g}^{(Q,l)}\Big|_{\text{MC}} = \frac{\alpha_s}{2\pi} \frac{d\xi_Q^{(l)}}{\xi_Q^{(l)}} dz_Q^{(l)} P_{qg}^{(0)}(z_Q^{(l)}) d\bar{\sigma}_{\gamma g} \Theta\left(1 - \xi_Q^{(l)}\right) \Theta\left((z_Q^{(l)})^2 - \frac{2m^2}{|\bar{t}_Q| \xi_Q^{(l)}}\right), \quad (12)$$

$$d\hat{\sigma}_{\gamma g}^{(\bar{Q},l)}\Big|_{\text{MC}} = d\hat{\sigma}_{\gamma g}^{(Q,l)}\Big|_{\text{MC}} \left(\bar{t}_Q \rightarrow \bar{t}_{\bar{Q}}, z_Q^{(l)} \rightarrow z_{\bar{Q}}^{(l)}, \xi_Q^{(l)} \rightarrow \xi_{\bar{Q}}^{(l)}\right). \quad (13)$$

- γq initial state

$$d\hat{\sigma}_{\gamma q}^{(+,u)}\Big|_{\text{MC}} = \frac{\alpha_{em}}{2\pi} \frac{d\xi_+^{(u)}}{\xi_+^{(u)}} dz_+^{(u)} P_{q\gamma}^{(0)}(z_+^{(u)}) d\bar{\sigma}_{\bar{q}q} \Theta\left((z_+^{(u)})^2 - \xi_+^{(u)}\right), \quad (14)$$

$$d\hat{\sigma}_{\gamma q}^{(-,t)}\Big|_{\text{MC}} = \frac{\alpha_s}{2\pi} \frac{d\xi_-^{(t)}}{\xi_-^{(t)}} dz_-^{(t)} P_{gq}^{(0)}(z_-^{(t)}) d\bar{\sigma}_{\gamma g} \Theta\left((z_-^{(t)})^2 - \xi_-^{(t)}\right). \quad (15)$$

- $\gamma\bar{q}$ initial state

$$d\hat{\sigma}_{\gamma\bar{q}}^{(+,t)}\Big|_{\text{MC}} = \frac{\alpha_{em}}{2\pi} \frac{d\xi_+^{(t)}}{\xi_+^{(t)}} dz_+^{(t)} P_{q\gamma}^{(0)}(z_+^{(t)}) d\bar{\sigma}_{\bar{q}q} \Theta\left((z_+^{(t)})^2 - \xi_+^{(t)}\right), \quad (16)$$

$$d\hat{\sigma}_{\gamma\bar{q}}^{(-,u)}\Big|_{\text{MC}} = \frac{\alpha_S}{2\pi} \frac{d\xi_-^{(u)}}{\xi_-^{(u)}} dz_-^{(u)} P_{gq}^{(0)}(z_-^{(u)}) d\bar{\sigma}_{\gamma g} \Theta\left((z_-^{(u)})^2 - \xi_-^{(u)}\right). \quad (17)$$

The Born cross sections $d\bar{\sigma}_{\gamma g}$, $d\bar{\sigma}_{\bar{q}q}$ or $d\bar{\sigma}_{\gamma g}^{(l)}$ have to be computed using the relevant definitions of \bar{s} , \bar{t} and \bar{u} , as explained in ref. [9]. One also defines [13]

$$d\bar{\sigma}_{\gamma g}^{(t)} = d\bar{\sigma}_{\gamma g} \frac{\bar{u}/\bar{t}}{\bar{u}/\bar{t} + \bar{t}/\bar{u}} = \frac{d\bar{\sigma}_{\gamma g}}{1 + \bar{t}^2/\bar{u}^2}, \quad d\bar{\sigma}_{\gamma g}^{(u)} = \frac{d\bar{\sigma}_{\gamma g}}{1 + \bar{u}^2/\bar{t}^2}. \quad (18)$$

We stress that eqs. (14) and (16) describe QED branchings. When inserted in the MC@NLO short-distance cross sections, they subtract an MC contribution which is generated when the hadronic-photon component is showered.

The situation of the contributions to the NLO expansion of PSMC cross sections is summarized in table 1.

	$q\bar{q} \rightarrow Q\bar{Q}$	$\bar{q}q \rightarrow Q\bar{Q}$	$\gamma g \rightarrow Q\bar{Q}$
γg			$-(t, u), Q(t, u), \bar{Q}(t, u)$
γq		$+(u)$	$-(t)$
$\gamma\bar{q}$	$+(t)$		$-(u)$

Table 1: Short-distance contributions to MC subtraction terms, from Born processes $q\bar{q} \rightarrow Q\bar{Q}$, $\bar{q}q \rightarrow Q\bar{Q}$, and $\gamma g \rightarrow Q\bar{Q}$. The three rows correspond to real-emission processes, identified by their incoming partons. Each entry lists the emitting legs (+, −, Q, \bar{Q}); for each emitting leg, we report in parentheses the different contributions l , according to the possible colour flows (which correspond to choosing $E_0^2 = |\vec{l}|/2$).

4. Comparisons to measurements of heavy-quark production at HERA

In this section the MC@NLO predictions will be compared to selected measurements of various observables relevant to the production of B and of $D^{*\pm}$ mesons, as reported by the H1 and ZEUS experiments. The quark masses and PDFs used by MC@NLO are given in table 2. The uncertainty band in MC@NLO is computed by varying the factorization and renormalization scales independently, by a factor of two up and down from the default scale $1/2(m_{Q,T} + m_{\bar{Q},T})$, and by taking the envelope of the results obtained in this way. For charm quarks these scales may become fairly small, and indeed charm production is pushing the applicability of perturbative QCD to its limits – this is one of the reasons why it is interesting to compare MC@NLO results for this process to data.

m_b	4.75 GeV
m_c	1.5 GeV
Proton PDF	Cteq6.6
Photon PDF	GRV

Table 2: Parameter settings used by MC@NLO.

In order to quantify the level of agreement between MC@NLO predictions and data, the quantity χ^2/ndf has been calculated for each data set, by taking into account both theory and experimental uncertainties. The relevant results are summarized in table 5 for bottom measurements, and in table 8 for charm measurements.

No effort has been made here to tune HERWIG (version 6.510) to HERA data, since the idea is that of making an out-of-the-box comparison. The only exception to this rule is an *overall* rescaling, applied to all hadron-level observables in order to have values of branching ratios consistent with those reported by the PDG [14] – these rescaling factors are equal to 1.34 and 1.5 for charm and bottom respectively.

4.1. *B-hadron production*

Bottom-flavoured hadrons are typically tagged by searching for the muons that arise from W 's, which in turn come from the weak decay of the lowest-lying b -hadrons into lighter-quark states. These muons will in general have a large momentum transverse to the jet axis, so called p_T^{rel} . Also, the vertex from which these muons are radiated will be displaced relative to the hard interaction of the event, and this displacement is proportional to the lifetime of the b -hadron. Often, only the transverse component δ of this displacement is used in the b -tagging. These two methods of tagging the b -quarks may be combined to further enhance the signal.

In this section, comparisons will be made with three measurements performed by H1 and ZEUS at HERA. They are:

1. “Measurement of beauty photoproduction using decays into muons in dijet events at HERA”, by the ZEUS collaboration [15];
2. “Measurement of beauty production at HERA using events with muons and jets”, by the H1 collaboration [16];
3. “Beauty photoproduction measured using decays into muons in dijet events in ep collisions at $\sqrt{s} = 318$ GeV”, by the ZEUS collaboration [17].

These will be referred to as ZEUS-09, H1-05 and ZEUS-03 respectively. The first two analyses use the combined method of both p_T^{rel} and δ in the tagging of the b -quarks, while in ZEUS-03 only p_T^{rel} is used. The experimental cuts made for the bottom analyses are summarized in table 3. These cuts result in the visible cross-sections listed in table 4, where also the MC@NLO predictions are shown; theory and data are in good agreement.

Analysis	ZEUS-09	H1-05	ZEUS-03
\sqrt{s}	318 GeV	318 GeV	318 GeV
Q^2	$< 1 \text{ GeV}^2$	$< 1 \text{ GeV}^2$	$< 1 \text{ GeV}^2$
y_{JB}	$0.2 - 0.8$	$0.2 - 0.8$	$0.2 - 0.8$
$p_t(\mu)$	$> 2.5 \text{ GeV}$	$> 2.5 \text{ GeV}$	$> 2.5 \text{ GeV}$
$\eta(\mu)$	$-1.6 - 1.3$	$-0.55 - 1.1$	$-1.48 - 2.3$
$p_T(\text{jet}_{1,2})$	7, 6 GeV	7, 6 GeV	7, 6 GeV
$\eta(\text{jet})$	$-2.5 - 2.5$	$-2.5 - 2.5$	$-2.5 - 2.5$

Table 3: A summary of the cuts relevant to the bottom analyses considered in this paper.

Visible σ [pb]	Measured	MC@NLO
ZEUS-09	$38.6^{+5.78}_{-6.02}$	42.08 ± 4.91
H1-05	38.4 ± 6.38	33.71 ± 2.89
ZEUS-03	50.25 ± 6.45	48.39 ± 3.87

Table 4: The visible cross sections within the cuts listed in table 3. The different measurements are compared to MC@NLO predictions.

ZEUS-09	MC@NLO
$p_T(\mu)$	0.18
$\eta(\mu)$	0.05
$x_\gamma(\text{jets})$	0.59
$\Delta\phi(\text{jets})$	1.22
$\Delta\phi(\text{jets}) x_\gamma^{\text{obs}} < 0.75$	0.52
H1-05	MC@NLO
$p_T(\mu)$	0.89
$\eta(\mu)$	0.11
$x_\gamma(\text{jets})$	0.48
ZEUS-03	MC@NLO
$p_T(\mu)$	0.78
$\eta(\mu)$	0.34
$p_T(b - \text{jet})$	0.09
$p_T(b)$	0.65
$x_\gamma(\text{jets})$	0.17

Table 5: The χ^2/ndf for all distributions in the bottom measurements shown in this paper.

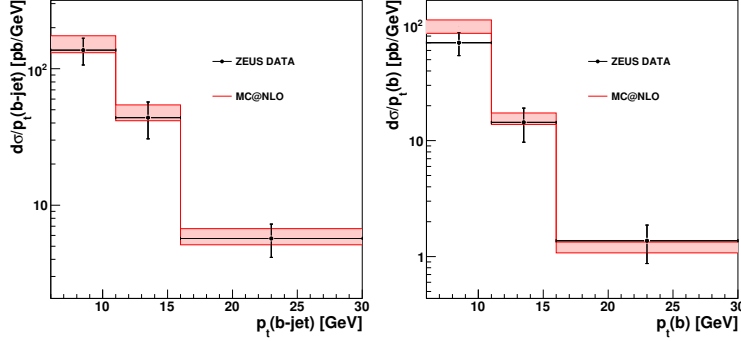


Figure 1: Distributions of $p_T(b - \text{jet})$ and $p_T(b)$ from the measurement ZEUS-03. The MC@NLO band includes full independent scale variations.

In fig. 1 the p_T of the jet containing a b -quark is shown, as measured in ZEUS-03. This spectrum is then used by the ZEUS collaboration to reconstruct the p_T spectrum of the b -quarks, using the NLO calculation FMNR [3]. Both distributions are well described by MC@NLO. The $p_T(b - \text{jet})$ prediction of MC@NLO, being at the hadron level, has been rescaled for the overall branching ratio factor as discussed before. On the other hand, the $p_T(b)$ spectrum, being a quantity at the parton level, has not been rescaled. It should be stressed that the use of NLO computations matched to parton showers implies that the deconvolution of data from hadron to parton level is not necessary for a fair comparison with theoretical predictions; in fact, such deconvolutions have to be deprecated, since they introduce unnecessary theoretical biases in the measurements (e.g., in the present case, the underlying matrix elements of FMNR and MC@NLO are the same; hence, the comparison done for $p_T(b)$ is not as significant as that for $p_T(b - \text{jet})$).

In fig. 2 the transverse momentum spectra of the tagged muons are shown. MC@NLO is describing all three data sets well for this observable. Also, the scale variations in MC@NLO are at the same level or smaller than the experimental uncertainties. The rapidity distributions of the muons are also well described by MC@NLO in all three data sets, as seen in fig. 3.

Two types of correlations have been measured for bottom production. One is the x_γ^{obs} distribution of the two leading jets in the measurements, shown in fig. 4. The variable x_γ^{obs} is defined by:

$$x_\gamma^{\text{obs}}(\text{jet}_1, \text{jet}_2) = \frac{P_-(\text{jet}_1) + P_-(\text{jet}_2)}{\sum_{\text{All hadrons } i} P_-(i)} \quad (19)$$

where $P_- = E - P_z$. Thus, x_γ^{obs} is the fraction of the measured hadronic P_- carried by the two leading jets, and at the LO it coincides with the fraction of the photon energy which enter into the hard interaction. Therefore, the hadronic part of the calculation is expected to be more important for small

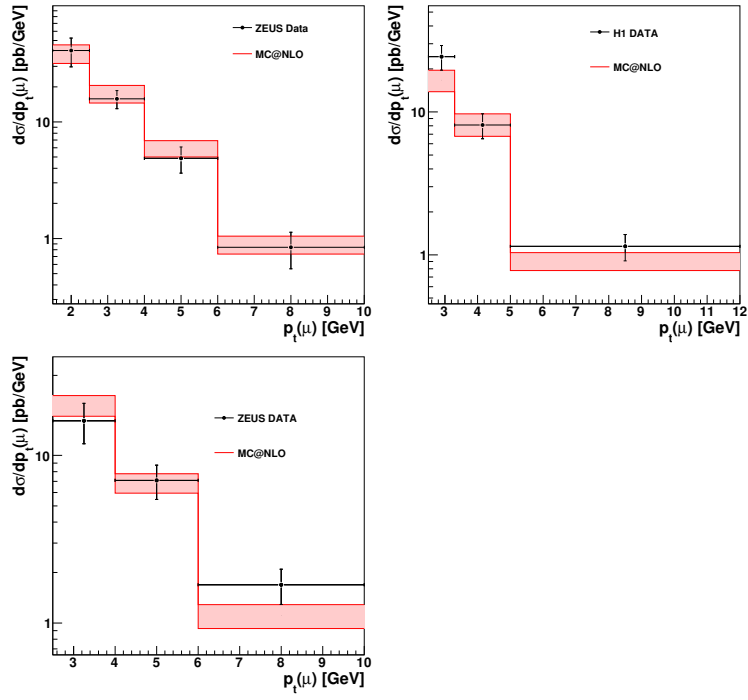


Figure 2: Distributions of $p_T(\mu)$ from the measurements ZEUS-09 (upper left), H1-05 (upper right) and ZEUS-03 (bottom). The MC@NLO band includes full independent scale variations.

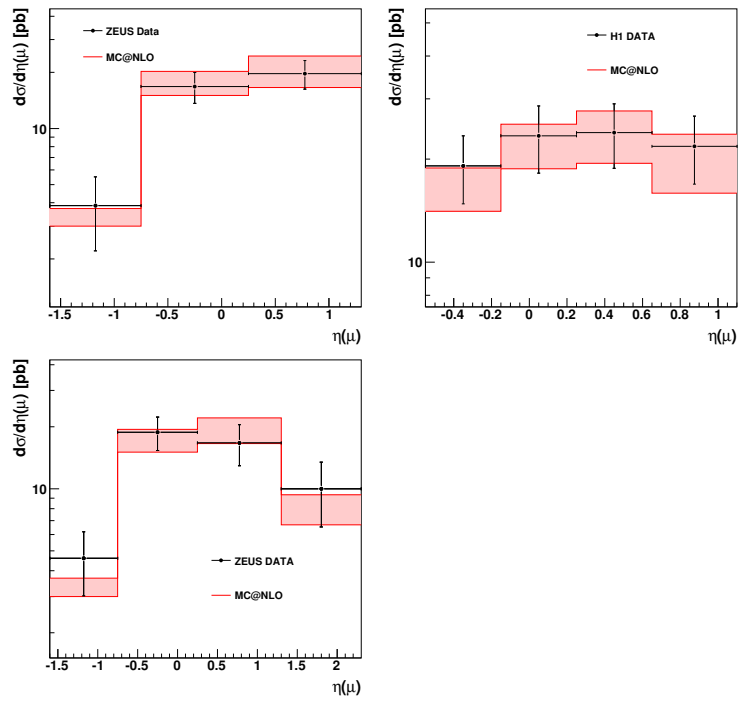


Figure 3: Distributions of $\eta(\mu)$ from the measurements ZEUS-09 (upper left), H1-05 (upper right) and ZEUS-03 (bottom). The MC@NLO band is obtained with independent scale variations.

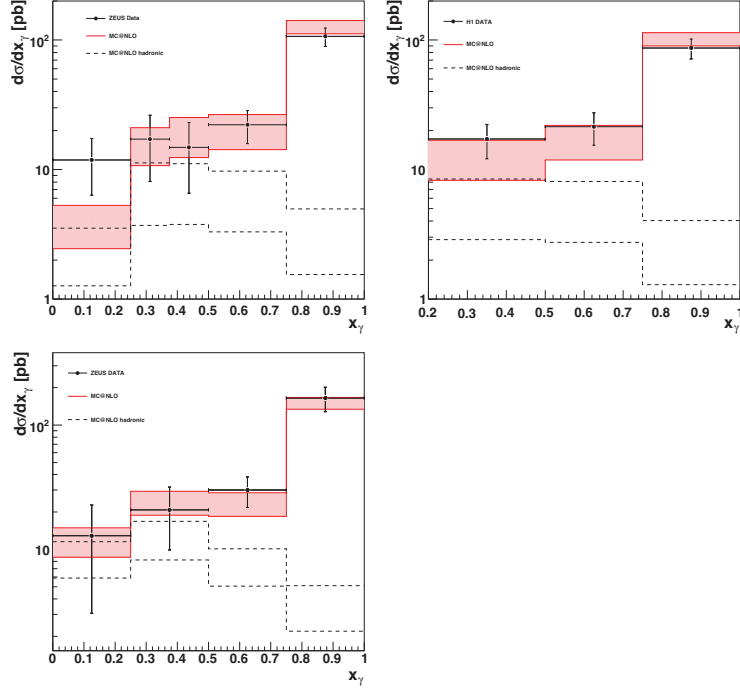


Figure 4: Distributions of x_{γ}^{obs} from the measurements ZEUS-09 (upper left), H1-05 (upper right) and ZEUS-03 (bottom). The MC@NLO band includes full independent scale variations.

values of x_{γ}^{obs} . MC@NLO describes all three measurements well. In these plots, the hadronic part of the MC@NLO calculation is also shown separate and, as expected, becomes significant for $x_{\gamma}^{\text{obs}} < 0.75$.

An observable which is highly sensitive to higher-order effects is the difference in azimuthal angle between the two leading jets. At $\Delta\phi \simeq \pi$ one observes the typical logarithmic divergence of infrared-sensitive variables computed at fixed-order in perturbation theory; this divergence is suppressed by the Sudakov damping, present in resummed computations and therefore naturally included in Monte Carlos. Multiple soft and collinear emissions are also relevant to small $\Delta\phi$ values (especially when rather small transverse momenta are involved), where however there are non-negligible contributions due to hard matrix elements, present in perturbative computations but not in ordinary PSMCs. It is therefore clear that MC@NLO, by incorporating both contributions, is expected to give a better description for this variable than either fixed-order computations or ordinary PSMCs. We present the comparison of MC@NLO predictions with data in fig. 5; the agreement is satisfactory, given the large experimental uncertainties. This observable is also presented by separating the large and small x_{γ}^{obs} regions, which are dominated by the pointlike and hadronic photon components

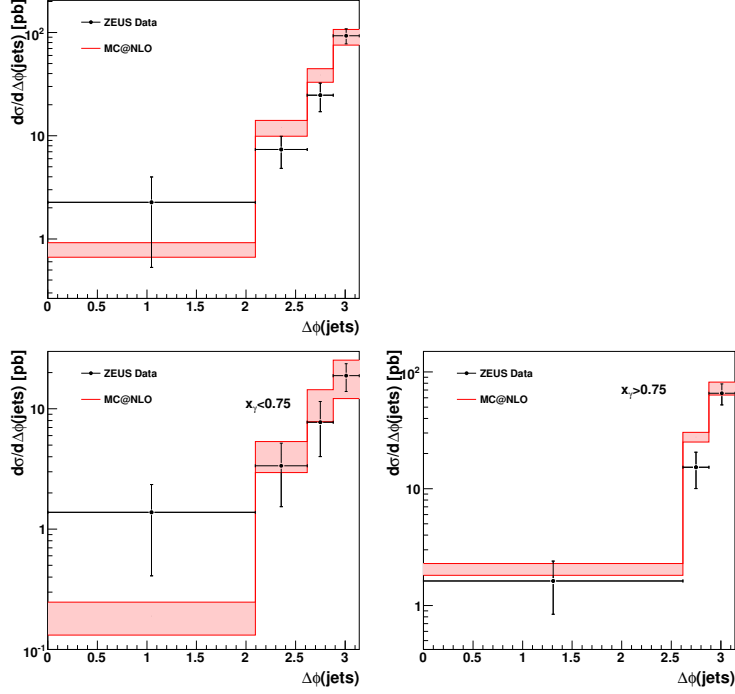


Figure 5: Distributions of $\Delta\phi(\text{jets})$, unbinned and binned in $x_{\gamma}^{\text{obs}}(\text{jets})$ from ZEUS-09. The MC@NLO band includes full independent scale variations.

respectively. The results are also displayed in fig. 5.

4.2. $D^{*\pm}$ production

The $D^{*\pm}$ mesons are detected through the so-called golden decay channel:

$$D^{*\pm} \rightarrow D^0 \pi_{\text{slow}}^{\pm} \rightarrow K^{\mp} \pi^{\pm} \pi_{\text{slow}}^{\pm}. \quad (20)$$

The branching ratio for the golden decay channel is $\sim 2.6\%$ [14], which is comparatively low, but the advantage of this channel is that all the final state particles carry an electric charge, resulting in three charged tracks in the detectors.

In this section MC@NLO will be compared to two $D^{*\pm}$ measurements. These are:

1. “Inclusive D^* -Meson Cross Sections and D^* -Jet Correlations in Photoproduction at HERA” by the H1 collaboration [18];
2. “Inclusive jet cross sections and dijet correlations in $D^{*\pm}$ photoproduction at HERA” by the ZEUS collaboration [19].

Analysis	H1-06	ZEUS-05
\sqrt{s}	318 GeV	318 GeV
Q^2	$< 0.01 \text{ GeV}^2$	$< 1 \text{ GeV}^2$
y_{JB}	$0.29 - 0.65$	$0.19 - 0.87$
$p_t(D^*)$	$> 2 \text{ GeV}$	$> 3 \text{ GeV}$
$\eta(D^*)$	$-1.5 - 1.5$	$-1.5 - 1.5$
$\eta(\text{jet})$	$-1.5 - 1.5$	$-1.5 - 2.4$
$p_T(\text{jet}_{1,2})$	4,3 GeV	

Table 6: A summary of the cuts in the D^* meson measurements.

Visible C-S [nb]	Measured	MC@NLO
H1-06 inclusive D^*	6.45 ± 0.83	6.45 ± 0.78
H1-06 $D^* + \text{jets}$	3.01 ± 0.44	2.88 ± 0.29
ZEUS-05	6.80 ± 0.26	5.77 ± 0.42

Table 7: The resulting visible cross-sections from the cuts listed in table 6, for the different measurements as well for the MC@NLO predictions. H1-06 consists of two measurements: of inclusive D^* and of $D^* + \text{jets}$. These are listed separately here.

These will be referred to as H1-06 and ZEUS-05 respectively. The experimental cuts applied in the D^* analyses are summarized in table 6. These cuts result in the visible cross sections reported in table 7, together with the theoretical predictions. MC@NLO describe the H1-06 measurements very well and is two sigma below the data for ZEUS-05.

4.2.1. Inclusive $D^{*\pm}$ production

In fig. 6 the $p_T(D^*)$ and $\eta(D^*)$ spectra are shown for inclusive D^* measurement. The H1-06 measurement is well described but the scale uncertainties in the MC@NLO prediction are rather large in comparison with the experimental uncertainties. In the $p_T(D^*)$ distributions, these scale uncertainties are reduced for larger $p_T(D^*)$, since the overall hardness of the process is increased. In fig. 6 the $\eta(D^*)$ distribution is also shown separately for $p_T(D^*) > 4.5 \text{ GeV}$, where the scales uncertainties in MC@NLO are at the same level as the experimental uncertainties. Here, two of the bins are well described, but the overall shape is not. However, given the very large uncertainties involved, the χ^2/ndf for this distribution is a mere 1.67.

4.2.2. $D^{*\pm}$ plus jet production

When demanding the tagging of a hard jet, as well as that of a $D^{*\pm}$ meson, the scale dependencies in MC@NLO are expected to be smaller than for inclusive variables, owing to the extra hardness of the jet. In fig. 7, the $p_T(D^*)$ and $\eta(D^*)$ distributions from the H1-06 measurements are shown, when events with a hard

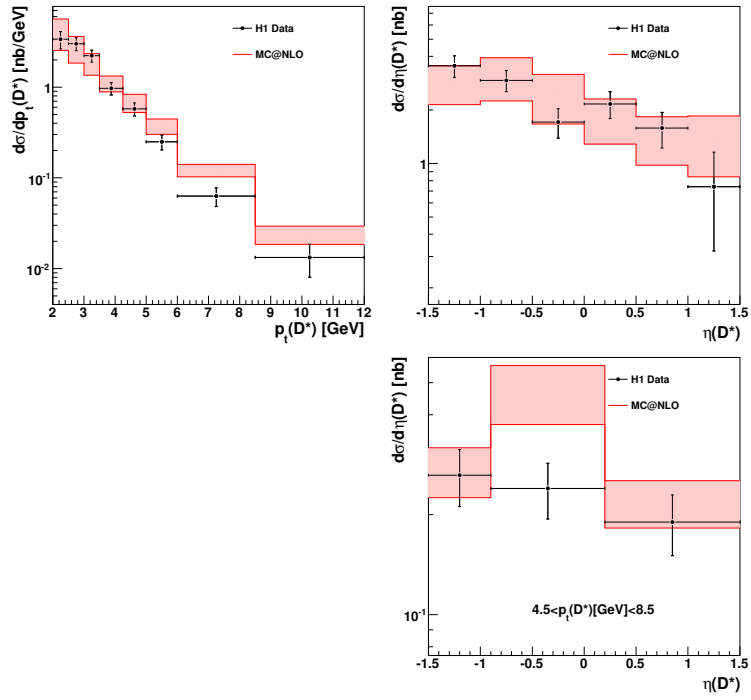


Figure 6: Distributions of $p_T(D^*)$ and $\eta(D^*)$ of inclusive D^* measurements H1-06. The MC@NLO band includes full independent scale variations.

H1-06 inclusive	MC@NLO χ^2/nds
$p_T(D^*)$	1.41
$\eta(D^*)$	0.46
$\eta(D^*) p_T(D^*) > 4.5 \text{ GeV}$	1.67
H1-06 $D^* + \text{jet}$	MC@NLO χ^2/nds
$p_T(D^*)$	2.49
$\eta(D^*)$	0.52
x_γ^{obs}	1.94
$\Delta\phi(D^*, \text{jet})$	0.67
$\Delta\eta(D^*, \text{jet})$	0.28
ZEUS-05	MC@NLO χ^2/nds
$p_T(D^*)$	0.94
x_γ^{obs}	1.05
$\Delta\phi(D^*, \text{jet})$	1.37
$p_T(\text{jj})$	1.01
M_{jj}	1.42
$\eta(\text{untagged jet}) p_T(\text{jet}) > 9 \text{ GeV}$	0.78

Table 8: The χ^2/ndf for all distributions in $D^{*\pm}$ -measurements shown.

jet with $p_T(\text{jet}) > 4 \text{ GeV}$ are chosen. The scale dependence is indeed reduced. The data are still well described, even though the $p_T(D^*)$ spectrum is a bit harder in MC@NLO than in the H1-06 data, while in ZEUS-05 ¹ the opposite is observed.

Also, correlations between D^* mesons and jets have been measured in H1-06 and ZEUS-05. In fig. 8, distributions in x_γ^{obs} are shown. One can see that the contribution by the hadronic part of MC@NLO is larger in the H1-06 measurement. However, MC@NLO is one sigma above the data for large x_γ^{obs} in this measurement, while the whole spectrum is well described in the ZEUS-05 measurement.

In fig. 9 the difference in azimuthal angle between the D^* meson and the hardest jet not containing the D^* (for H1-06), and between the two hardest jets in a D^* event (for ZEUS-05) are shown. One can see that MC@NLO describes the data over the whole $\Delta\phi$ spectrum for both analyses, something fixed order NLO calculations cannot do (see e.g. fig. 9 in ref. [18], and fig. 11 in ref. [19]).

Another observable which is sensitive to higher order effects is the p_T of the two leading jets, which was measured in ZEUS-05, and shown here in fig. 10. In this figure, the distribution of the invariant mass of the two jets is also presented.

¹This $p_T(D^*)$ distribution is not presented in ref. [19]. We have compiled it from other distributions binned in $p_T(D^*)$.

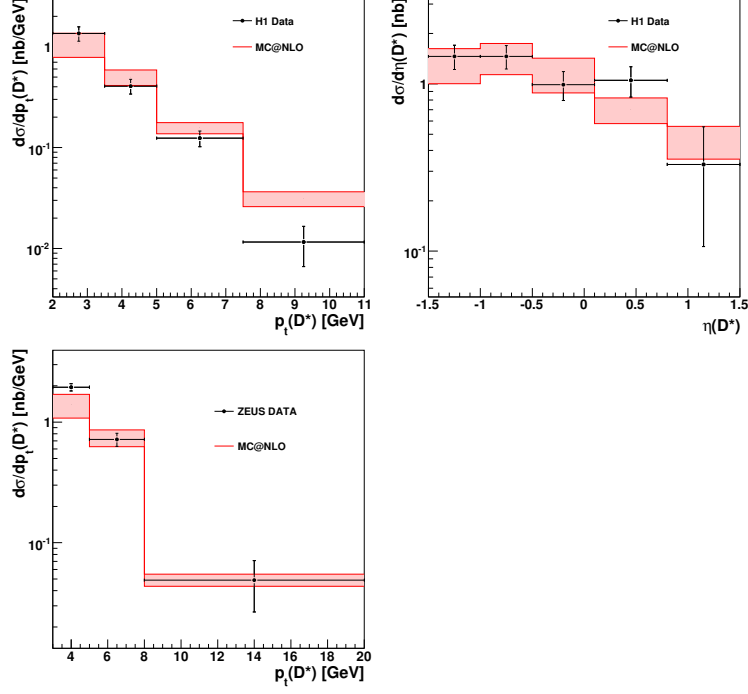


Figure 7: Distributions of $p_T(D^*)$ and $\eta(D^*)$ in the $D^* + \text{jets}$ measurements from H1-06 as well as $p_T(D^*)$ from ZEUS-05. The MC@NLO band includes full independent scale variations.

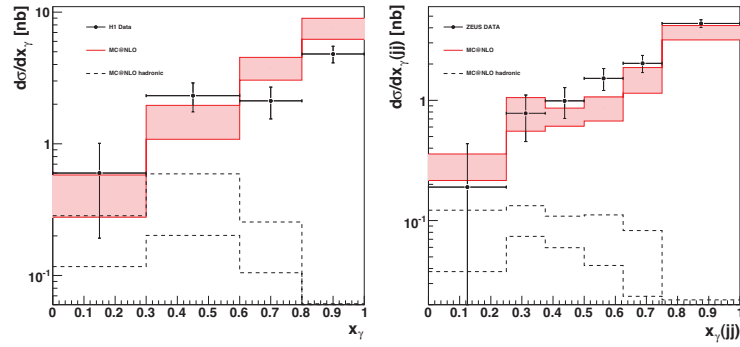


Figure 8: Distributions of $x_\gamma^{\text{obs}}(\text{jets})$ from H1-06 (left) and ZEUS-05 (right). The MC@NLO band includes full independent scale variations.

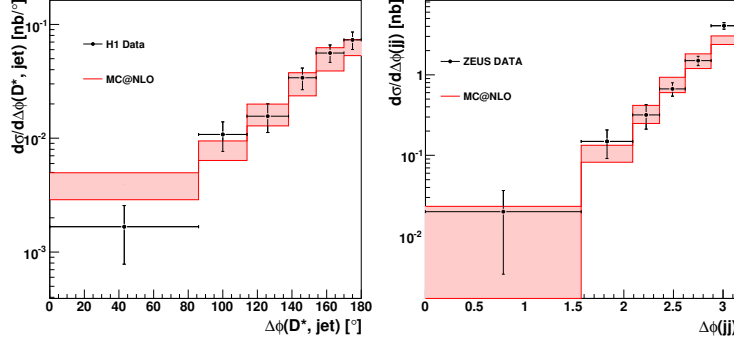


Figure 9: Distributions of $\Delta\phi$ from H1-06 (left) and ZEUS-05 (right). The MC@NLO band includes full independent scale variations.

MC@NLO is seen to describe both these observables in a reasonable manner. Also, the difference in pseudo-rapidity between the D^* and the hardest other jet is sensitive to higher order radiations. This was measured in H1-06 as shown in the bottom plot of fig. 10. MC@NLO is describing the spectrum in $\Delta\eta(D^*, \text{jet})$ very well, with $\chi^2/ndf = 0.28$.

5. Conclusions

In this letter, we have applied the MC@NLO formalism to the pointlike photoproduction of heavy-quark pairs. Together with the already-available $Q\bar{Q}$ hadroproduction code, this has been employed to carry out a comparison between theoretical predictions and the data collected by the H1 and ZEUS experiments at HERA, relevant to b - and c -hadron observables.

In particular, MC@NLO has been compared to five sets of measurements, three for b -flavoured hadrons, and two for c -flavoured hadrons. All data have been shown to be described within one standard deviation by MC@NLO. It should be pointed out that MC@NLO predictions are absolute, except for an overall rescaling needed to obtain a branching ratio into muons (in the case of bottom production), and into D^* 's (in the case of charm production) compatible with the world averages.

Although the overall agreement between theory and data appears to be satisfactory, it should be kept in mind that the uncertainties involved are sometimes quite large. For bottom production, theoretical errors are at the same level or smaller than experimental ones. On the other hand, for charm production the largest uncertainties are those of MC@NLO, and therefore the comparisons carried out here only loosely constrain perturbative QCD predictions. The situation improves when hard jets are also part of the observable definitions.

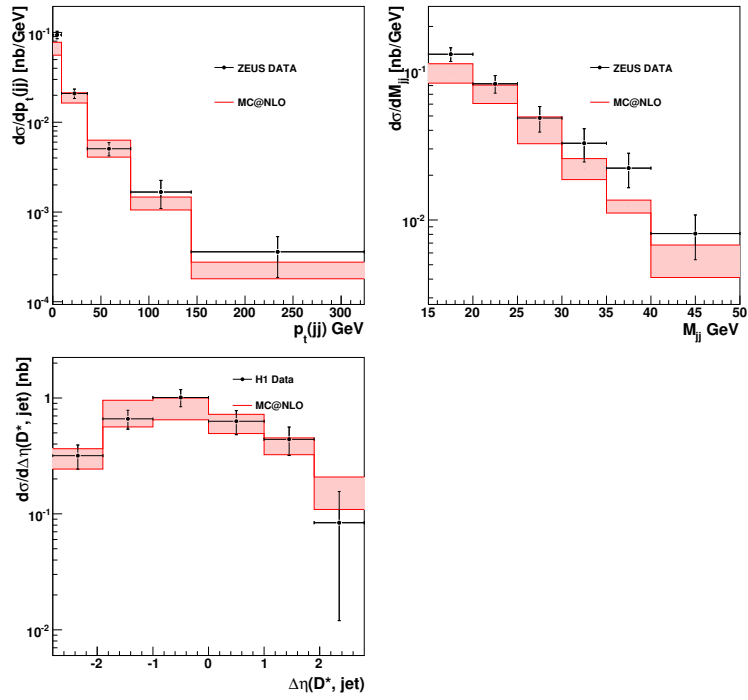


Figure 10: Distributions of $p_T(jj)$ and M_{jj} from ZEUS-05 and of $\Delta\eta(D^*, \text{jet})$ from H1-06. The MC@NLO band includes full independent scale variations.

6. Acknowledgements

The authors would like to thank Bryan Webber and Hannes Jung for great help and useful discussions. T.T. was supported by DESY and by Hamburg University. S.F. is on leave of absence from INFN, Sezione di Genova, Italy.

References

- [1] Z. J. Ajaltouni *et al.*, “Proceedings of the workshop: HERA and the LHC workshop series on the implications of HERA for LHC physics,” arXiv:0903.3861 [hep-ph].
- [2] B. W. Harris and J. Smith, “Charm quark and D^{*+} cross-sections in deeply inelastic scattering at HERA,” Phys. Rev. D **57** (1998) 2806 [arXiv:hep-ph/9706334].
- [3] S. Frixione, M. L. Mangano, P. Nason and G. Ridolfi, “Heavy quark correlations in photon - hadron collisions,” Nucl. Phys. B **412** (1994) 225 [arXiv:hep-ph/9306337].
- [4] G. P. Salam, “Elements of QCD for hadron colliders,” arXiv:1011.5131 [].
- [5] S. Frixione and B. R. Webber, “Matching NLO QCD computations and parton shower simulations,” JHEP **0206** (2002) 029 [hep-ph/0204244].
- [6] C. F. von Weizsacker, Z. Phys. **88** (1934) 612.
- [7] E. J. Williams, Phys. Rev. **45** (1934) 729.
- [8] S. Frixione, M. L. Mangano, P. Nason and G. Ridolfi, Phys. Lett. B **319** (1993) 339 [arXiv:hep-ph/9310350].
- [9] S. Frixione, P. Nason and B. R. Webber, “Matching NLO QCD and parton showers in heavy flavour production,” JHEP **0308** (2003) 007 [arXiv:hep-ph/0305252].
- [10] G. Marchesini, B. R. Webber, G. Abbiendi, I. G. Knowles, M. H. Seymour and L. Stanco, “HERWIG: A Monte Carlo event generator for simulating hadron emission reactions with interfering gluons. Version 5.1 - April 1991,” Comput. Phys. Commun. **67** (1992) 465.
- [11] G. Corcella, I.G. Knowles, G. Marchesini, S. Moretti, K. Odagiri, P. Richardson, M.H. Seymour and B.R. Webber, “HERWIG 6: An event generator for hadron emission reactions with interfering gluons (including supersymmetric processes),” JHEP **0101** (2001) 010 [hep-ph/0011363].
- [12] G. Corcella *et al.*, “HERWIG 6.5 release note,” arXiv:hep-ph/0210213.
- [13] K. Odagiri, “Color connection structure of supersymmetric QCD ($2 \rightarrow 2$) processes,” JHEP **9810** (1998) 006 [arXiv:hep-ph/9806531].

- [14] K. Nakamura *et al.* [Particle Data Group], “Review of particle physics,” J. Phys. G **37**, 075021 (2010).
- [15] S. Chekanov *et al.* [ZEUS Collaboration], “Measurement of beauty photoproduction using decays into muons in dijet events at HERA,” JHEP **0904**, 133 (2009). [arXiv:0901.2226 [hep-ex]].
- [16] A. Aktas *et al.* [H1 Collaboration], “Measurement of beauty production at HERA using events with muons and jets,” Eur. Phys. J. **C41**, 453-467 (2005). [hep-ex/0502010].
- [17] S. Chekanov *et al.* [ZEUS Collaboration], “Beauty photoproduction measured using decays into muons in dijet events in e p collisions at $s^{*1/2} = 318\text{-GeV}$,” Phys. Rev. **D70**, 012008 (2004). [hep-ex/0312057].
- [18] A. Aktas *et al.* [H1 Collaboration], “Inclusive D^{*+} - Meson Cross Sections and D^{*+} - Jet Correlations in Photoproduction at HERA,” Eur. Phys. J. **C50**, 251-267 (2007). [hep-ex/0608042].
- [19] S. Chekanov *et al.* [ZEUS Collaboration], “Inclusive jet cross sections and dijet correlations in D^{*+} - photoproduction at HERA,” Nucl. Phys. **B729**, 492-525 (2005). [hep-ex/0507089].